

The effect of cobalt addition to bulk MoP and Ni₂P catalysts for the hydrodesulfurization of 4,6-dimethyldibenzothiophene

Ibrahim I. Abu, Kevin J. Smith*

Department of Chemical & Biological Engineering, University of British Columbia, 2360 East Mall, Vancouver, BC, Canada, V6T 1Z3

Received 1 March 2006; revised 1 May 2006; accepted 3 May 2006

Available online 12 June 2006

Abstract

Bulk metal phosphide catalysts with nominal composition Co_xNi₂P ($0 \leq x \leq 0.34$) and Co_{0.07}MoP were investigated for the hydrodesulfurization (HDS) of 4,6-dimethyldibenzothiophene (4,6-DMDBT) at 583 K and 3.0 MPa H₂. The selectivity for the direct desulfurization (DDS) of 4,6-DMDBT to the product dimethylbiphenyl (DMBP) increased to 49 and 31% over the Co_{0.08}Ni₂P and Co_{0.07}MoP catalysts, respectively, compared with the <3% DMBP selectivity obtained on bulk Ni₂P and MoP. Analysis by X-ray photoelectron spectroscopy (XPS) showed that the addition of the Co to MoP and Ni₂P resulted in a P enrichment of the catalyst surface. Among the Co_xNi₂P and Co_{0.07}MoP catalysts studied, the maximum DMBP selectivity occurred for the Co_{0.08}Ni₂P catalyst; this catalyst had the highest *n*-propylamine uptake and lowest CO uptake and the highest P/metal atom ratio, as determined by XPS. The increased selectivity to DMBP suggests that acid sites associated with phosphorous promote skeletal isomerization of 4,6-DMDBT to yield products that readily undergo DDS on the metal sites of the Co_xNi₂P ($0 \leq x \leq 0.34$) and Co_{0.07}MoP catalysts.

© 2006 Elsevier Inc. All rights reserved.

Keywords: Hydrodesulfurization; Metal phosphide; Cobalt; Catalyst; 4,6-Dimethyldibenzothiophene

1. Introduction

Hydrotreating is an important crude oil refining process that removes S, N, and O from hydrocarbon molecules by reacting them with H₂ over a catalyst. Conventional hydrotreating catalysts, sulfides of Co–Mo, Ni–Mo, and Ni–W supported on alumina, have been extensively studied and reviewed [1,2]. New catalysts described in the literature for hydrodesulfurization (HDS) and hydrodenitrogenation (HDN) include metal carbides and nitrides [3–7] and, more recently, metal phosphides [8–14]. In some studies, metal phosphides have been shown to be more active than conventional metal sulfides for HDS [15,16] and HDN [12,17]. The transition metal monophosphides (M/P = 1) and metal-rich phosphides (M/P > 1) are of the greatest interest in hydrotreating catalysis because of their superior stability compared with phosphorous-rich (M/P < 1) metal phosphides [8]. Both bulk and supported metal phosphides can be

prepared by the temperature-programmed reduction (TPR) of the corresponding metal phosphates [13–21].

The hydrotreating activities of monophosphides (MoP and WP), metal-rich phosphides (Co₂P and Ni₂P), and ternary phosphides (CoMoP and NiMoP) have been reported in a number of studies [9,12,14,18]. Oyama [14] reported that for the metal phosphides, HDS activity, measured for the HDS of dibenzothiophene (DBT) and reported per mole of CO uptake, increased in the order Fe₂P < CoP < MoP < WP < Ni₂P. The catalysts showed almost complete selectivity to the direct desulfurization (DDS) product, biphenyl. Furthermore, the activities of Ni_xP_y catalysts supported on SiO₂ were shown to be dependent on the Ni/P ratio, and the most active catalyst had an initial Ni/P ratio of 1/2, which decreased to 1/0.57, or Ni₂P_{1.14}, after 100 h of reaction. The effect of P was much more profound for HDN than for HDS; Oyama et al. [22] suggested that HDS must therefore occur on metal centers. Ni₂P/SiO₂ catalysts were also shown to be more effective in removing S from refractory compounds, such as 4-methyldibenzothiophene and 4,6-dimethyldibenzothiophene (4,6-DMDBT) than a conventional Co–Mo–S/Al₂O₃ catalyst [16]. The ability of Ni₂P

* Corresponding author. Fax: +1 604 822 6003.
E-mail address: kjs@interchange.ubc.ca (K.J. Smith).

to selectively remove S without excessive hydrogenation of the aromatic ring was suggested to be due to the exposure of many crystallite corners and edges.

The activity of monophosphides and metal-rich phosphides is not increased by the addition of a second metal, such as Co or Ni [17,18,23,24]. Zuzaniuk and Prins [17] and Stinner et al. [18] reported that the ternary phosphides, CoMoP and NiMoP, prepared such that the Co/Mo and Ni/Mo ratios were 1/1, had activities for HDN of *o*-propylaniline less than those of MoP and Co₂P catalysts. Sun et al. [23] reported that increased Ni content in a Ni–Mo–P catalyst resulted in increased activity for HDS of DBT, but observed no synergistic effect between the Ni and Mo and found that Ni₂P had higher activity than all of the Ni–Mo–P catalysts tested. They concluded that Ni was not a promoter of HDS in the Ni–Mo–P system either. Similarly, Rodriguez et al. [24] showed that a NiMoP/SiO₂ catalyst was much less active than either MoP/SiO₂ or Ni₂P/SiO₂ for the HDS of thiophene.

The rate of HDS of the refractory compound 4,6-DMDBT is typically an order of magnitude lower than that of thiophene or DBT. HDS of thiophenic compounds proceeds by hydrogenolysis of the C–S bond (referred to as direct desulfurization, DDS) or by hydrogenation of the aromatic ring followed by hydrogenolysis (the hydrogenation route, HYD). The desulfurization rate of 4,6-DMDBT via the HYD route is much higher than that by DDS on CoMoS/Al₂O₃ catalysts [31]. Steric hindrance by the methyl groups at the 4- and 6-positions of the DBT skeleton hinders the access of S to the active site. Isoda et al. [31] showed that the HDS of 2,8-DMDBT has a lower apparent activation energy and is 5–10 times more reactive (depending on temperature) than 4,6-DMDBT over CoMoS/Al₂O₃ catalyst. Consequently, one potential option to increase the rate of 4,6-DMDBT HDS is to isomerize the molecule such that the methyl groups migrate to positions that eliminate steric hindrance. For example, Kwak et al. [30] reported that addition of P to CoMoS/Al₂O₃ catalyst increased the Brønsted acidity and promoted migration of the methyl groups of 4,6-DMDBT such that more DMBP was produced than MCHT.

In the present study we report on the beneficial effect of adding low concentrations of Co to Ni₂P and MoP catalysts in the HDS of 4,6-DMDBT. Few studies of 4,6-DMDBT HDS over metal phosphides are available, and in previous studies of ternary phosphides, the catalysts were prepared such that the M/P ratio was fixed. In this study, Co is added to Ni₂P and MoP (without additional P) to obtain increasingly metal-rich phosphides, with their nominal composition represented by Co_xNi₂P and Co_yMoP. Bulk phosphides have been studied initially to avoid support effects, especially related to the acid properties of the catalysts.

2. Experimental

2.1. Catalyst preparation

The Co_xNi₂P catalysts were prepared by dissolving stoichiometric amounts (Ni/P = 2/1) of nickel nitrate [Ni(NO₃)₂·6H₂O, Aldrich, 99% purity] and diammonium hydrogen phos-

phate [DAHP; (NH₄)₂HPO₄, Sigma, 99% purity] in a beaker containing 15 mL of deionized water. The resulting solution was stirred at room temperature while adding 10 mL of a cobalt nitrate solution, prepared by dissolving an appropriate amount of cobalt nitrate hexahydrate [(Co(NO₃)₂·6H₂O, Acros] in 10 mL of deionized water to give the desired mol% Co in the final Co_xNi₂P catalyst. After addition of the cobalt solution, the mixture was stirred while evaporating to dryness. The material was further dried in an oven at 373 K for 2 h and calcined at 773 K for 6 h. The calcined product (or Co_xNi₂P precursor) was ground to a powder (*d*_p < 0.7 mm) and subjected to temperature-programmed reduction (TPR) in H₂ (Praxair, 99.99%) at a flow rate of 120 ml(STP)/min and a temperature ramp rate of 1 K/min to a final temperature of 1000 K. The final temperature was maintained for 2 h. After the reduction, the catalyst was cooled to room temperature in He at a flow rate of 20 ml/min. Before removal from the reactor, the Co_xNi₂P was passivated in 2% O₂/He for 2 h at room temperature. The Co_{0.07}MoP was prepared similarly using ammonium heptamolybdate [(NH₄)₆Mo₇O₂₄·4H₂O, AnalaR(BDH), 99% purity], DAHP, and Co(NO₃)₂·6H₂O to give 3.2 mol% Co in MoP. The mixture was treated thermally as before, except that the reduction temperature was increased to 1200 K.

The catalysts were compared with bulk Co₂P, CoP, MoP, and Ni₂P prepared using stoichiometric amounts of Co(NO₃)₂·6H₂O and (NH₄)₂HPO₄ in the case of CoP and Co₂P, stoichiometric amounts of (NH₄)₆Mo₇O₂₄·4H₂O and (NH₄)₂HPO₄ in the case of MoP, and stoichiometric amounts (Ni/P = 2/1 molar ratio) of nickel nitrate [Ni(NO₃)₂·6H₂O] and (NH₄)₂HPO₄ in the case of Ni₂P. All solutions were treated thermally as before, although because of the absence of the cobalt nitrate solution, the initial drying (crystallization) time was much shorter for the monophosphides than for Co_xNi₂P and Co_yMoP.

2.2. Catalyst characterization

TPR of the catalyst precursors was conducted in a 60-mL/min flow of 10% H₂ in Ar using 0.2–0.4 g of the calcined sample loaded into a stainless steel reactor (9 mm i.d.). A thermal conductivity detector (TCD) was used to measure the H₂ consumption as the reactor was heated at 1 K/min to the final temperature of 1000 or 1200 K. The reactor was maintained at this temperature for 2 h before cooling to 313 K at a rate of 5 K/min. The TCD response was calibrated by reducing a known amount Cu₂O under the same conditions.

The mass change of the catalyst during TPR was also measured for the CoP, Ni₂P, and Co_{0.08}Ni₂P catalyst using a tapered element oscillating microbalance (TEOM Series 1500 Pulsed Mass Analyzer; Rupprecht and Patashnick), with the catalyst in a fixed-bed configuration and continuous gas flow through the bed during the mass measurement. About 0.2 g of catalyst was placed in the reactor and heated in He (UHP, Praxair) at a flow rate of 60 mL(STP)/min and 393 K for 2 h before cooling to room temperature. The reduction in H₂ followed using a purge He (UHP, Praxair) flow of 120 mL(STP)/min and a pure H₂ (UHP, Praxair) flow of 120 mL(STP)/min. The temperature was ramped at 1 K/min to 979 K, holding at this temperature

for 2 h before cooling to room temperature. The single-point BET surface area of the catalysts was measured using a Micro-metrics FlowSorbII 2300. About 1 g of passivated catalyst was degassed at 393 K for 2 h, and the measurement was made using 70% He and 30% N₂.

Powder X-ray diffraction (XRD) analyses were performed on the passivated catalysts using a Siemens D500 Cu-K α X-ray source of wavelength 1.54 Å. The analysis was performed using a 40-kV source, a scan range of 3°–70° with a step size of 0.04°, and a step time of 2 s. The phase identification was carried out after subtraction of the background using standard software. Crystallite size estimates were made using the Scherrer equation, $d_c = K\lambda/\beta \cos\theta$, where the constant K is taken to be 0.9, λ is the wavelength of radiation, β is the peak width in radians, and θ is the angle of diffraction.

Transmission electron microscope images (TEM) were generated using a Fei Tecnai 20 scanning transmission electron microscope operating at 200 kV. STEM-EDX analysis was conducted using the same instrument. Catalyst samples were ground to a fine powder, dispersed in ethanol, and sonicated for 10 min. A drop of the catalyst suspension was placed on a 200-mesh copper grid coated with Formvar and carbon and left to dry before analysis.

The CO uptake was measured using pulsed chemisorption. About 0.5–1.0 g of catalyst was pretreated in a stainless steel reactor (9 mm i.d.) to remove the passivation layer by passing 60 mL/min of 10% H₂ in Ar while heating from 313 to 723 K at a rate of 2 K/min, maintaining the final temperature for 1 h. The reactor was then cooled to 298 K in a flow of H₂. An He flow at 30 mL/min was used to flush the catalyst for 30 min to achieve an adsorbate-free, reduced catalyst surface. After pretreatment, 1-mL pulses of CO were injected into a flow of He (30 mL/min), and the CO uptake was measured using a TCD. CO pulses were repeatedly injected until the response from the detector showed no further CO uptake after consecutive injections, and the total CO uptake, reported herein in units of $\mu\text{mol}/\text{m}^2$, was obtained by dividing the uptake in $\mu\text{mol}/\text{g}$ by the measured BET area. Assuming a 1:1 adsorption stoichiometry between CO and metal atoms, this value corresponds to the metal site density on the catalyst surface.

The catalyst Brønsted acid sites were titrated by *n*-propylamine (*n*-PA) temperature-programmed desorption using the same reactor and TCD used for the CO chemisorption. A flow of He (30 mL/min) saturated at room temperature with *n*-propylamine (Aldrich, 99.8%) was passed through heated gas lines to the reactor containing about 1 g of catalyst that had been pretreated as before. After 2 h of adsorption at 383 K, the reactor was flushed in pure He at a flow rate of 30 mL/min for 1 h to ensure removal of physically adsorbed *n*-PA. The chemisorbed *n*-PA was then desorbed by ramping the reactor temperature from 383 to 973 K at a rate of 5 K/min, and the TCD was used to quantify the amount of *n*-PA desorbed. The system was calibrated using three zeolite samples of known acidity.

A Leybold Max200 X-ray photoelectron spectrometer was used for XPS studies. Al-K α was used as the photon source for all of the metal phosphides except the Co_{*x*}Ni₂P phosphide, for which Mg-K α was used because of the Ni(A) overlap with

the Co 2p peak when the former is used as the X-ray source. Both Al-K α and Mg-K α radiation was generated at 15 kV and 20 mA. The pass energy was set at 192 eV for the survey scan and at 48 eV for the narrow scan. All catalyst samples were analyzed after passivation at room temperature. Exposure of the samples to ambient atmosphere was minimized by transferring the samples either in vacuum or under nitrogen (UHP). All XPS spectra were corrected to the C 1s peak at 285.0 eV.

The HDS of 4,6-DMDBT was carried out in a fixed-bed reactor (9 mm i.d.) at 583 K and 3.0 MPa H₂. The 4,6-DMDBT at a concentration of 3000 ppm was dissolved in dodecane and fed to the reactor using a Gilson Model 0154E metering pump. Before entering the reactor, the liquid was evaporated into the stream of flowing H₂. Gas and liquid flows and catalyst charged to the reactor were chosen to give a WHSV of 0.6 h⁻¹. The passivated catalysts ($d_p < 0.7$ mm) were activated at 723 K for 2 h in H₂ at a flow rate of 160 mL(STP)/min. The temperature was then cooled to the reaction temperature of 583 K, and the reaction was initiated using the appropriate feed flow conditions. The product was collected periodically and analyzed using a 3400 GC Varian Star gas chromatograph equipped with a flame ionization detector (FID). Component separation was achieved using a capillary column (CP-Sil 19 CB, 25 m long and 0.53 mm i.d.). Component identification was confirmed using the same column and a gas chromatograph–mass spectrometer (Agilent 6890/5973N). In two cases, sulfur speciation among components of the product was also measured using an HP6890 gas chromatograph equipped with a G2350A AED detector and a RESTEK 10526 crossbond 50% methylpolysiloxane column. In this case, component identification was confirmed by a TOF mass spectroscopy. These analyses were conducted at the National Center for Upgrading Technology, Devon, Alberta.

A carbon balance between the reactor feed and effluent showed closures of >95% for all of the catalyst activity data reported herein.

3. Results

3.1. Catalyst properties

XRD analysis of the calcined catalyst precursors showed the Co_{0.07}MoP precursor to be amorphous, whereas NiO was identified in the Co_{*x*}Ni₂P precursors, in agreement with similar observations made for MoP and Ni₂P precursors [15]. The results suggest that after calcination, Ni was in the +2 oxidation state and Mo was likely in the +6 oxidation state [17], although the presence of other, amorphous species cannot be excluded [11].

The XRD patterns of the reduced catalysts, shown in Figs. 1 and 2, were used to identify the crystalline phases present and to estimate the lattice parameters. The crystallite size (d_c) was calculated using the Scherrer equation (Table 1). In all cases, the diffractograms showed that metal phosphides had been successfully prepared. No metal oxide or metal phosphate species were detected by XRD. The XRD data for the Co_{*x*}Ni₂P catalysts (Table 1), with $0 \leq x \leq 0.16$ (i.e., up to 5.1 mol% Co)

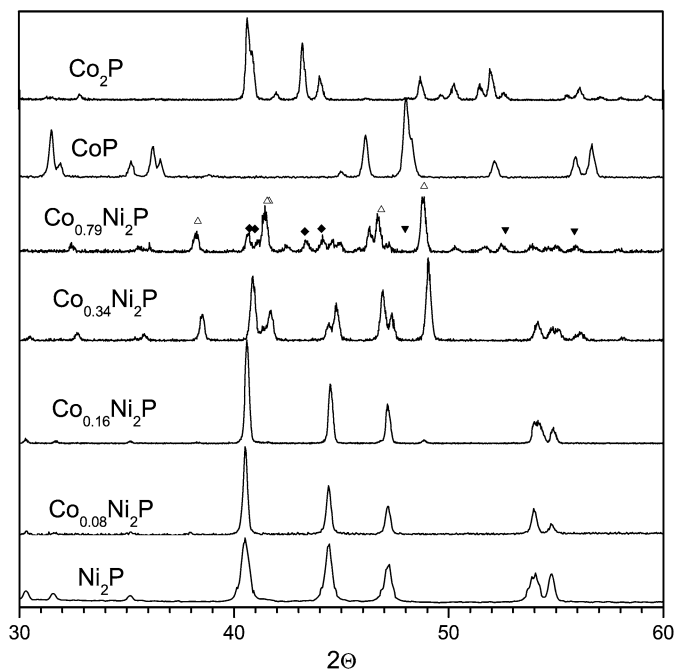


Fig. 1. X-ray diffractograms of reduced Co_2P , CoP and $\text{Co}_x\text{Ni}_2\text{P}$ catalysts ((Δ) Ni_{12}P_5 , (\blacklozenge) Co_2P , (\blacktriangledown) NiCoP).

showed the presence of Ni_2P with no significant difference in the Ni_2P lattice parameters ($a = 0.5877 \pm 0.0003$ nm and $c = 0.3412 \pm 0.0008$ nm). For $x \geq 0.34$, the $\text{Co}_x\text{Ni}_2\text{P}$ showed the development of the metal-rich phosphides Ni_{12}P_5 and Co_2P , in addition to Ni_2P . The Ni_2P lattice parameters decreased ($a = 0.5862 \pm 0.0002$ nm and $c = 0.3375 \pm 0.0021$ nm), although the error associated with the estimate of the lattice parameter c increased for these catalysts, because the XRD diffractograms were a composite of a number of different phases (Fig. 1) and the (111) peak of Ni_2P was not well resolved. Co (0.152 nm) and Ni (0.149 nm) have very similar atomic radii, so that even if a solid solution were present for $\text{Co}_x\text{Ni}_2\text{P}$ with $x \leq 0.16$, the expected increase in the lattice parameter c would be within the measurement error of the powder XRD data.

The XRD pattern of the $\text{Co}_{0.07}\text{MoP}$ was very similar to that obtained for MoP and did not show characteristic CoP

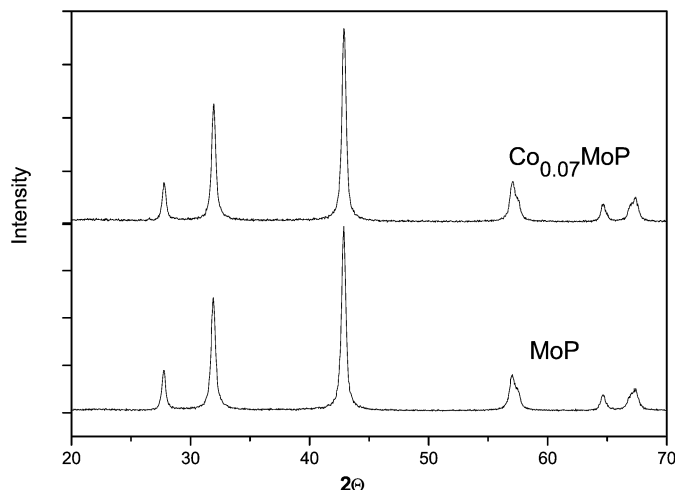


Fig. 2. X-ray diffractograms of reduced MoP and $\text{Co}_{0.07}\text{MoP}$ catalysts.

peaks, because the Co concentration was too low (3.2 mol% Co) and/or because Co was well dispersed in the MoP . The data in Table 1 show that the presence of Co resulted in a decrease in the lattice parameter c of MoP , suggesting that in this case a Co_xMoP solid solution was formed, as has been reported for the $\text{Ni}_x\text{Mo}_{(1-x)}\text{P}$ system [18,23,25].

The addition of Co to MoP and Ni_2P increased the MoP and Ni_2P crystallite size (Table 1), and the BET surface area also increased (Table 3). The bulk MoP or Ni_2P catalysts had low BET area (S_{BET}) and large particle size ($d_{\text{Ni}_2\text{P}} = 206$ nm and $d_{\text{MoP}} = 172$ nm, estimated from $d_p = 6/[S_{\text{BET}}\rho]$ where ρ is the bulk density). The particle size was significantly greater than the crystallite dimensions (d_c) shown in Table 1, suggesting significant agglomeration of the metal phosphide crystallites. The increased Ni_2P and MoP crystallite size with the addition of Co to Ni_2P and MoP was likely due to the increased time for complete crystallization compared with Ni_2P , because of the added $\text{Co}(\text{NO}_3)_2$ solution. The increased BET surface area of $\text{Co}_x\text{Ni}_2\text{P}$ and $\text{Co}_{0.08}\text{MoP}$ suggests a reduction in the degree of agglomeration of the larger crystallites when the Co was added.

Fig. 3 compares TEM micrographs of the Ni_2P and $\text{Co}_{0.08}\text{Ni}_2\text{P}$ bulk catalysts. The TEM images of Ni_2P and $\text{Co}_{0.08}\text{Ni}_2\text{P}$

Table 1
Lattice parameters estimated from PXRD of reduced catalysts

Catalyst	Co content (mol%)	Phases	Ni_2P phase							
			2θ ($^\circ$)				Lattice parameters (nm)		Crystallite size (nm)	
			(111)	(201)	(210)	(300)	a	c		
Ni_2P	0	Ni_2P	40.52	44.44	47.16	54.00	0.5879	0.3417	21	
$\text{Co}_{0.08}\text{Ni}_2\text{P}$	2.5	Ni_2P	40.52	44.40	47.20	53.96	0.5879	0.3417	36	
$\text{Co}_{0.16}\text{Ni}_2\text{P}$	5.1	Ni_2P	40.60	44.48	47.14	54.16	0.5874	0.3403	39	
$\text{Co}_{0.34}\text{Ni}_2\text{P}$	10.3	Ni_2P , Ni_{12}P_5	40.88	44.76	47.32	54.16	0.5860	0.3360	32	
$\text{Co}_{0.79}\text{Ni}_2\text{P}$	21.0	Ni_2P , Ni_{12}P_5 , Co_2P	40.66	44.59	—	—	0.5863	0.3389	27	
Catalyst	Co content (mol%)	Phases	MoP phase					Lattice parameters (nm)		Crystallite size (nm)
			2θ ($^\circ$)				a	c		
			(100)	(101)					d_c (100)	
MoP	0	MoP	31.93	42.89			0.3240	0.3196	16	
$\text{Co}_{0.07}\text{MoP}$	3.2	MoP	31.93	42.96			0.3240	0.3179	15	

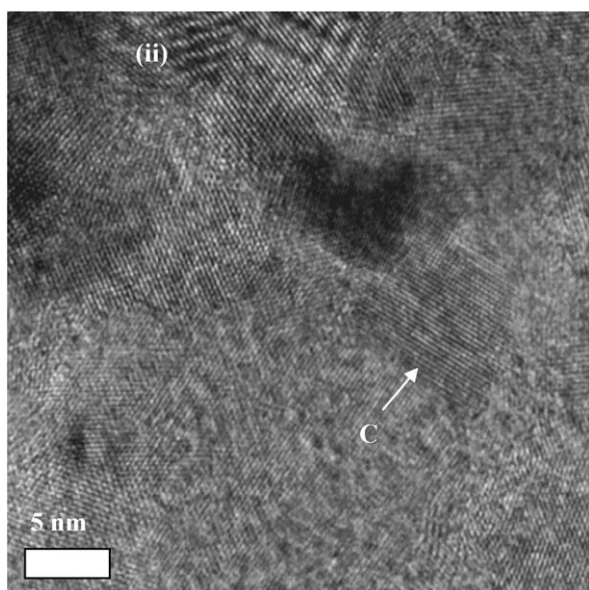
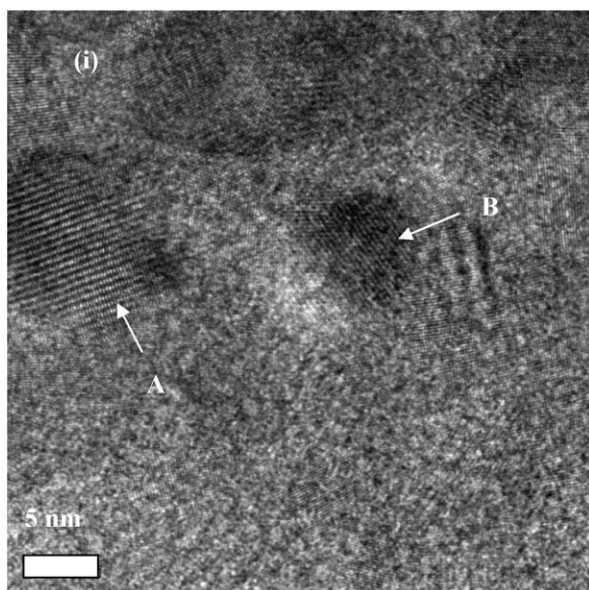


Fig. 3. TEM micrographs of bulk metal phosphides: (i) Ni_2P and (ii) $\text{Co}_{0.07}\text{-Ni}_2\text{P}$. Estimated d -spacing of lattice fringes shown are (A) 5.0, (B) 3.4 and (C) 2.8 Å corresponding to (100), (001) and (011) planes of Ni_2P .

are similar and show a mosaic crystal structure. Crystal planes with d -spacings estimated at 5.0, 3.4, and 2.8 Å, corresponding to the (100), (001), and (011) planes of Ni_2P can be identified. A multipoint STEM-EDX analysis of the $\text{Co}_{0.08}\text{Ni}_2\text{P}$ catalyst (nominal) yielded the composition $\text{Co}_{0.16 \pm 0.12}\text{Ni}_{2.00 \pm 0.12}\text{P}_{1.08 \pm 0.13}$, indicative of a uniform catalyst composition. In the case of the $\text{Co}_{0.34}\text{Ni}_2\text{P}$, however, a wider variation in composition was obtained ($\text{Co}_{0.15 \pm 0.18}\text{Ni}_{2.00 \pm 0.24}\text{P}_{0.11 \pm 0.17}$), consistent with the presence of different phases identified by XRD.

TPR profiles of the catalyst precursors are presented in Figs. 4 and 5. The two reduction peaks associated with the Ni_2P precursor are attributed to low-temperature reduction of NiO to Ni , followed by reduction of the phosphate to Ni_2P at higher temperature [15]. A similar TPR profile was observed for Co_2P . For $\text{Co}_x\text{Ni}_2\text{P}$ with $x \leq 0.16$, increasing Co con-

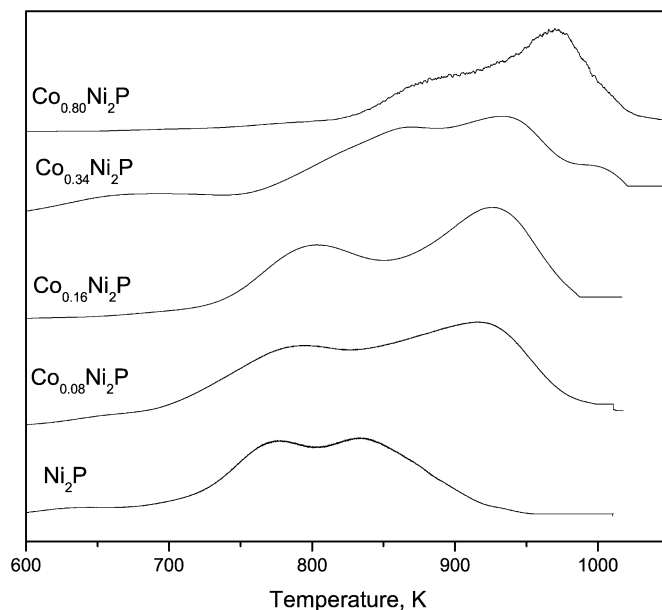


Fig. 4. TPR of Ni_2P and $\text{Co}_x\text{Ni}_2\text{P}$ catalyst precursors measured in 10% H_2 in Ar at a rate of 60 ml(STP)/min.

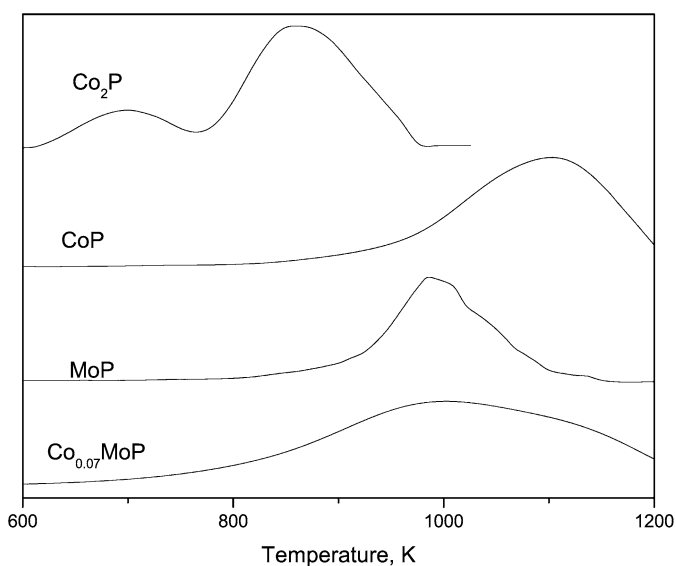


Fig. 5. TPR of Co_2P , CoP , MoP and $\text{Co}_{0.07}\text{MoP}$ catalyst precursors measured in 10% H_2 in Ar at a rate of 60 ml(STP)/min.

centration increased the temperature of the second maximum, most likely because of the high reduction temperature of the CoP precursor (1173 K) [17]. As the Co content increased further such that $x \geq 0.34$, both peak temperatures increased significantly, suggesting the formation of different reduced species, consistent with the XRD data that showed the presence of new phases (especially Ni_{12}P_5) in the reduced $\text{Co}_x\text{Ni}_2\text{P}$ catalysts with $x \geq 0.34$.

The TPR of the MoP precursor shows a peak at 955 K. Previous studies of the preparation of MoP supported on SiO_2 found two reduction peaks at about 720 and 1090 K [17]. The lower-temperature peak was attributed to Mo^{6+} reduction to Mo^{4+} , with subsequent Mo^{4+} and P^{5+} reduction occurring at

Table 2
Summary of temperature programmed reduction data

Catalyst	TPR peak temperature (K)	Assumed reduction stoichiometry	Apparent degree of reduction (mol%)	Weight loss	
				Calculated from reduction degree (wt%)	Measured using TEOM (wt%)
Ni ₂ P	778, 840	4NiO·P ₂ O ₅ + 9H ₂ → 2Ni ₂ P + 9H ₂ O	72	24	31
Co _{0.08} Ni ₂ P	785, 921	2CoO·P ₂ O ₅ + 7H ₂ → 2CoP + 7H ₂ O	74	25	51
		4NiO·P ₂ O ₅ + 9H ₂ → 2Ni ₂ P + 9H ₂ O			
MoP	955	2MoO ₃ ·P ₂ O ₅ + 11H ₂ → 2MoP + 11H ₂ O	62	25	–
Co _{0.07} MoP	1001	2CoO·P ₂ O ₅ + 7H ₂ → 2CoP + 7H ₂ O	66	25	–
		2MoO ₃ ·P ₂ O ₅ + 11H ₂ → 2MoP + 11H ₂ O			
CoP	1086	2CoO·P ₂ O ₅ + 7H ₂ → 2CoP + 7H ₂ O	46	18	24

higher temperatures. In the present work, the single broad peak at 955 K is assigned to the reduction of Mo⁶⁺ and P⁵⁺. The addition of 3.2 mol% Co to MoP resulted in a similar peak maximum temperature, although the TPR profile broadened compared with the MoP profile.

TPR data were also used to estimate the degree of reduction. However, the stoichiometry of the reduction reaction is difficult to determine, because, as pointed out by Stinner et al. [12], the catalyst precursors may include polyphosphate chains. Furthermore, Oyama et al. [15] have shown that under certain conditions, some phosphate species volatilize. Assuming that the species present after calcination can be written as $n\text{MO}_x \cdot \text{P}_2\text{O}_5$ [12], the degree of reduction calculated in Table 2 suggests that the precursors were not completely reduced to the metal phosphide. However, if the precursors included species such as $\text{H}_x\text{PO}_4^{(x-3)}$ or P^{3+} , the actual degree of reduction would be higher than that calculated. Similarly, if some unreduced, volatile phosphorous species were to leave the catalyst during the reduction or calcination process, then the actual degree of reduction would be higher than that calculated in Table 2. Support for the latter case is provided by the mass loss measurements made during TPR using the TEOM and reported in Table 2. The measured mass loss was greater than that calculated using the assumed stoichiometry and the measured H₂ consumption, indicative of the presence of other forms of oxide and/or phosphate species that must be present and not accounted for in the reduction stoichiometry.

Properties of the prepared catalysts, including the *n*-PA uptake and the CO uptake, reported per unit BET area of the catalyst, are summarized in Table 3. These data show that the CoP had the highest *n*-PA uptake among all metal phosphides examined. The *n*-PA uptake on Co_{*x*}Ni₂P with $x \leq 0.16$ was greater than on Ni₂P. The *n*-PA uptake increased by about 50% on Co_{0.07}MoP compared with MoP. The CO uptake decreased for the Co_{0.07}MoP and the Co_{0.08}Ni₂P catalysts compared with MoP and Ni₂P, respectively; however, for the Co_{*x*}Ni₂P catalysts, the CO uptake increased with increasing Co content of the Co_{*x*}Ni₂P catalysts. Excluding CoP, the catalysts with the highest *n*-PA uptake, Co_{0.07}MoP and Co_{0.08}Ni₂P, also had the lowest CO uptake.

The XPS spectra of the P 2p region, the Co 2d region, the Mo 3d region, and the Ni 2p region obtained on the various cat-

Table 3
Properties of the prepared metal phosphides

Catalyst	BET area (m ² /g)	Chemisorption		P/M ^a atom ratio	
		CO uptake (μmol/m ²)	<i>n</i> -PA uptake (μmol/m ²)	Nominal	XPS
Ni ₂ P	4.1	0.27	5	0.50	0.5
Co _{0.08} Ni ₂ P	7.9	0.11	18	0.48	4.8
Co _{0.16} Ni ₂ P	7.8	0.22	7	0.46	1.8
Co _{0.34} Ni ₂ P	6.9	0.42	1	0.43	1.2
Co _{0.79} Ni ₂ P	6.5	0.45	1	0.36	–
MoP	5.3	0.21	8	1.00	1.0
Co _{0.07} MoP	11.4	0.19	13	0.94	1.3
CoP	2.3	0.42	37	1.00	2.5
Co ₂ P	5.6	0.16	11	0.5	1.6

^a M: total metals (Co + Ni) or (Co + Mo) and P: phosphorous.

alysts are shown in Figs. 6 and 7. Note that these catalysts had not been re-reduced before the XPS analysis, as was done in the case of CO adsorption and *n*-PA adsorption. The P 2p_{3/2} binding energy (BE) has been reported to be 129.5 eV for the metal phosphides [19,20], 135.2–135.6 eV for P₂O₅ [26,27], and 133.3 eV for Ni₃(PO₄)₂ [28]. Hence we assign the low BE peak at 129.5–129.8 eV, present in the Co₂P, CoP, Ni₂P, and MoP spectra, to the metal phosphide, and the higher BE peak at 133.4–133.8 eV to surface metal phosphate species. For Ni₂P, this assignment is consistent with the Ni 2p BEs demonstrating the presence of Ni₂P and Ni₃(PO₄)₂ with corresponding Ni 2p_{3/2} BEs of 853.7 and 857.3 eV, respectively. A similar conclusion can be drawn for the Co₂P and CoP catalysts, with Co 2p BEs at 780.0–778.6 eV and 793.8 eV, and the MoP catalyst, with a Mo 3d BEs at 228.2 and 232.2 eV.

The effect of increasing Co content on the XPS spectra of the Co_{*x*}Ni₂P catalysts is also shown in Figs. 6 and 7. No significant shift in BE was observed in the case of P 2p_{3/2}, whereas in the case of Ni 2p, a feature at lower BE (852.7 eV) assigned to metal-rich phosphide (Ni₁₂P₅) [32] increased with increasing Co content. This observation is consistent with the presence of Ni₁₂P₅ identified by XRD in the Co_{*x*}Ni₂P catalysts with $x \geq 0.34$. In addition, as Co content increased, the peak assigned to phosphate species became less significant and the peak at 855.9 eV, assigned to Ni²⁺, increased. These results are consistent with those of Sawhill et al. [32], who reported that Ni₁₂P₅ is oxidized more readily during passivation

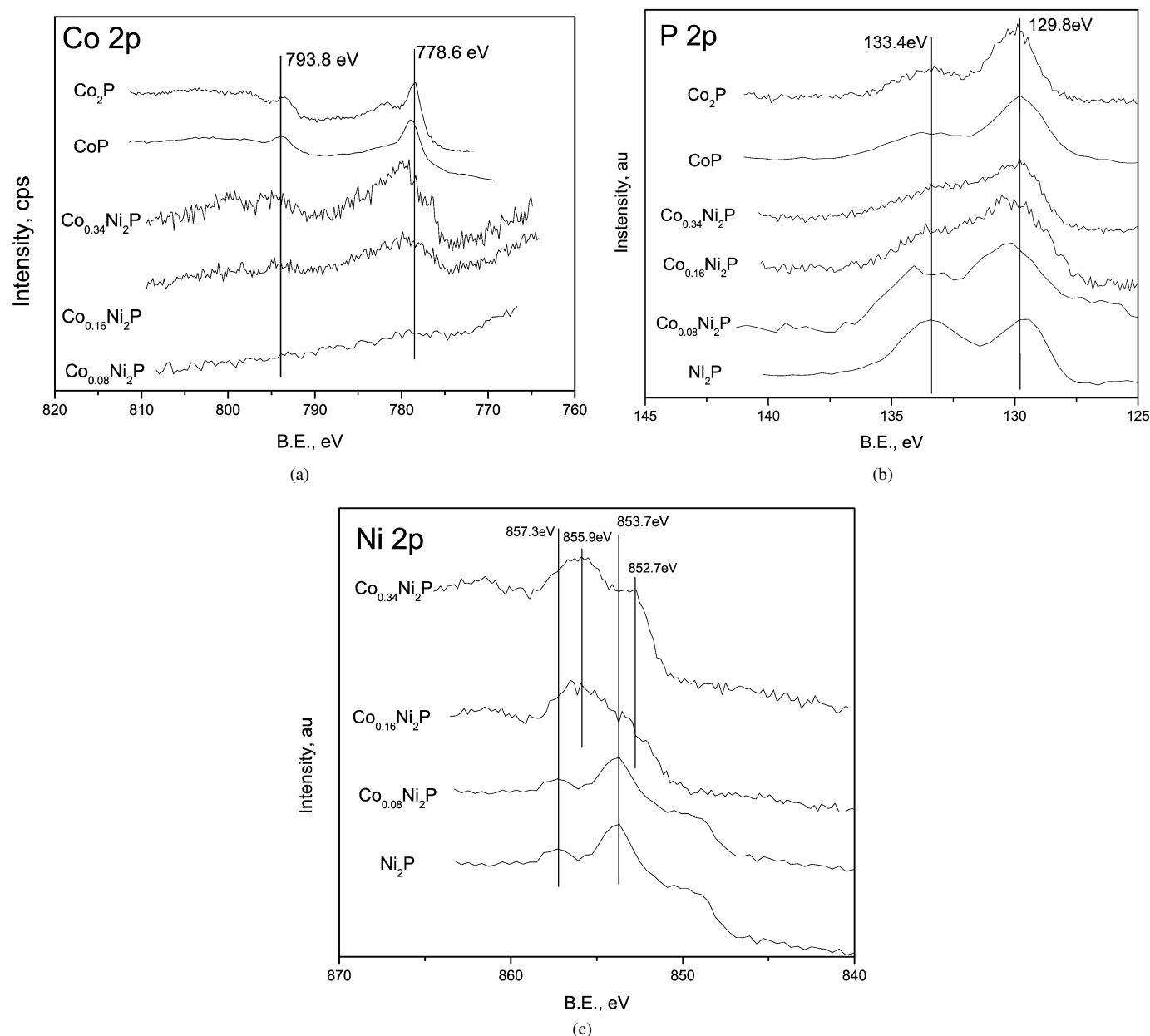


Fig. 6. XPS of (a) Co 2p region, (b) P 2p region, and (c) Ni 2p region of Co_xNi₂P catalysts after reduction and passivation.

than Ni₂P. The feature at ~850 eV is likely the L3VV Auger line of NiO [35]. Comparing the Co 2p peaks present in CoP and Co_xNi₂P (at BE = 780 eV) suggests the presence of metal phosphide, although there is a shift to lower BE of about 1.5 eV in the case of Co₂P, indicative of a more metallic Co species. In the case of Co_{0.07}MoP, the Mo 3d_{5/2} and P 2p_{3/2} BEs are almost identical to those observed in the case of MoP.

XPS analyses were also used to calculate the P/M atom ratios of the catalysts before their use. These data, given in Table 3, suggest that the surface of the MoP catalyst was slightly enriched in P, and that adding Co resulted in a small increase in surface P content. In the case of Ni₂P, the surface P/Ni ratio was close to 1/2, but after Co addition, a P surface enrichment occurred that was most significant for the Co_{0.08}Ni₂P catalyst [P/(Co + Ni) = 4.8].

Fig. 8 shows a correlation between the XPS and chemisorption data obtained on the metal phosphides of the present study. Assuming that the CO chemisorption titrates metal sites and the *n*-PA uptake titrates Brønsted acid sites, presumably associated with the surface phosphate species, the P/M atom ratio as determined by XPS should correlate with the *n*-PA to CO uptake ratio as determined by adsorption. The data plotted in Fig. 8 confirm the correlation ($R^2 = 0.88$), with some deviation associated with experimental error of the measured ratios indicated on the graph.

3.2. Catalyst activity

Before performing activity measurements, the passivated catalysts were reactivated in a H₂ flow at 723 K for 1 h. Catalyst

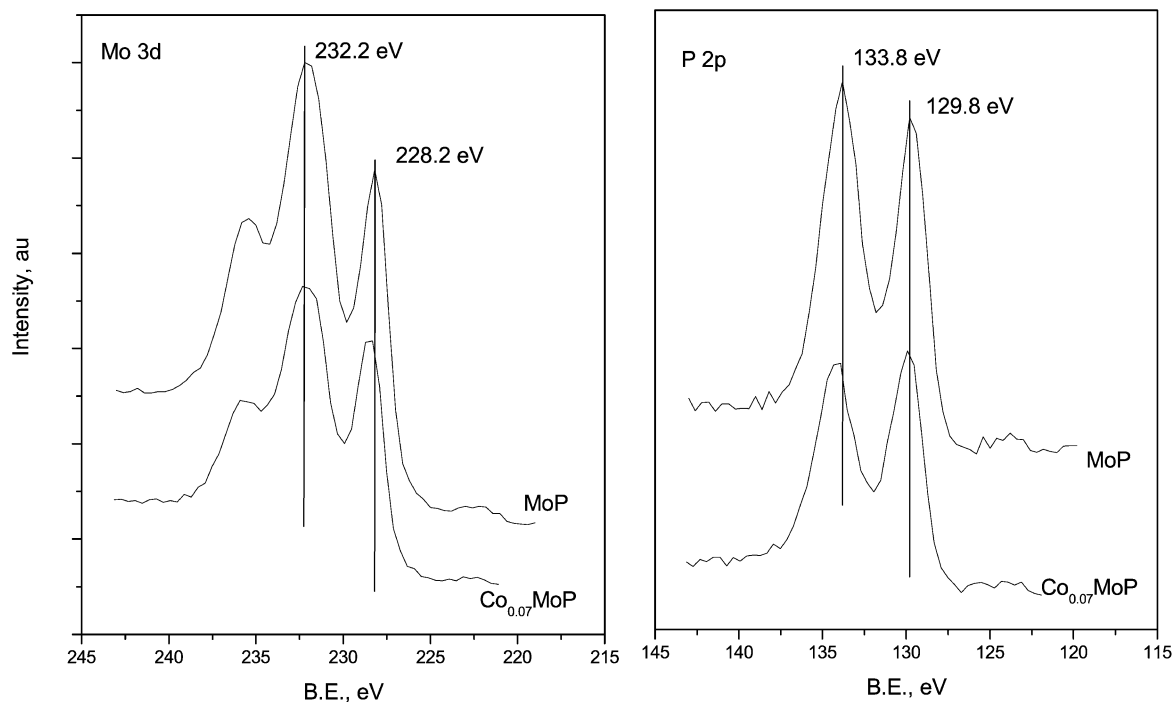


Fig. 7. XPS of P 2p region and Mo 3d region of MoP and $\text{Co}_{0.07}\text{MoP}$ catalysts after reduction and passivation.

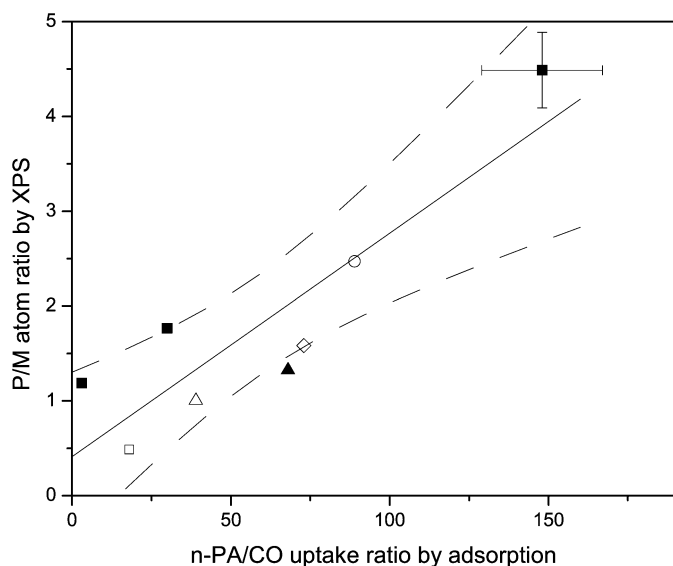


Fig. 8. Correlation of P/M ratio determined by XPS and $n\text{-PA/CO}$ uptake ratio determined by adsorption for $\text{Co}_x\text{Ni}_2\text{P}$ (■), $\text{Co}_{0.08}\text{MoP}$ (▲), CoP (○), Co_2P (◇) with MoP (△) and Ni_2P (□) as indicated. The solid line represents the correlation equation: $\text{P/M ratio} = (0.024 \pm 0.005) \times (n\text{-PA/CO uptake ratio}) + (0.411 \pm 0.364)$ and the dashed lines represent the 95% confidence limits of the correlation.

conversion data were then measured; the conversions typically reached a steady value after about 8 h time on stream. The conversion and selectivity data reported in Table 4 and Fig. 9 are the time-averaged values over a period of at least 4 h that followed the initial 8-h stabilization period. In each case, the complete product analysis was used to calculate product selectivities. A carbon balance between the reactor feed and reactor effluent was $>95\%$ for all the data reported herein.

The metal phosphides had conversions in the range 10–48 mol%, and by assuming that the conversion of 4,6-DMDBT on these catalysts was zero order at the conditions of the present study, the rate of 4,6-DMDBT consumption for each catalyst was calculated (Table 4). The specific rate (i.e., rate per gram of catalyst) increased on the $\text{Co}_{0.08}\text{Ni}_2\text{P}$ catalyst but declined on the $\text{Co}_x\text{Ni}_2\text{P}$ catalysts with $x \geq 0.16$, compared with Ni_2P . However, the data of Table 4 show that per unit area (BET), the activities of all the $\text{Co}_x\text{Ni}_2\text{P}$ catalysts were lower than those for the Ni_2P , Co_2P , and CoP catalysts, whereas the TOF based on CO uptake showed a maximum value for the $\text{Co}_{0.08}\text{Ni}_2\text{P}$ catalyst. Similar behavior was observed on the MoP catalyst versus the $\text{Co}_{0.07}\text{MoP}$ catalyst, except that the TOF was greater on the MoP catalyst than on the $\text{Co}_{0.07}\text{MoP}$ catalyst.

The major products of 4,6-DMDBT conversion, determined by gas chromatography–mass spectroscopy, were dimethylbicyclohexane (DMBCH), dimethylbiphenyl (DMBP), and methylcyclohexyltoluene (MCHT), with less significant quantities of hydrocarbons that were products of 4,6-DMDBT hydrocracking and hydrogenation. The selectivity of the catalysts to MCHT, DMBCH, and DMBP is reported in Table 4, with the remaining products being hydrogenated S-containing products or cracked products. The data show that with 4,6-DMDBT, hydrogenation products were favored over Ni_2P and MoP , in contrast to the high selectivity to DDS products occurring for DBT conversion over Ni_2P and MoP [15,23]. The low selectivity to DDS products in the case of 4,6-DMDBT is known to be due to steric hindrance by the methyl groups of the molecule. Of particular significance in the present work, however, is the increase in selectivity toward DMBP that occurred when Co was added to both the MoP and Ni_2P catalysts, especially at low Co content. An increase in DMBP selectivity suggests a signifi-

Table 4
Activities of bulk metal phosphides for the HDS of 4,6-DMDBT measured at 583 K and 3.0 MPa H₂

Catalyst	Conversion (mol%)	4,6-DMDBT consumption rate			Selectivity (mol%)		
		Specific (10 ⁹ mol/(g s))	Areal (10 ¹⁰ mol/(m ² s))	TOF (10 ³ s ⁻¹)	MCHT	DMBCH	DMBP
Ni ₂ P	29.1	2.06	5.01	1.87	2.1	25.7	0.9
Co _{0.08} Ni ₂ P	48.7	3.44	4.36	3.82	0.8	13.3	57.3
Co _{0.16} Ni ₂ P	23.4	1.65	2.12	0.95	14.6	10.5	40.9
Co _{0.34} Ni ₂ P	17.4	1.23	1.78	0.42	28.6	4.0	22.2
Co _{0.79} Ni ₂ P	10.1	0.71	1.10	0.25	25.1	5.7	16.3
MoP	36.2	2.56	4.83	2.33	32.1	1.4	1.2
Co _{0.07} MoP	42.5	3.00	2.63	1.41	10.7	1.3	46.9
CoP	22.3	1.58	6.85	1.62	17.8	12.0	2.3
Co ₂ P	43.9	3.10	5.54	3.52	15.7	21.6	33.3

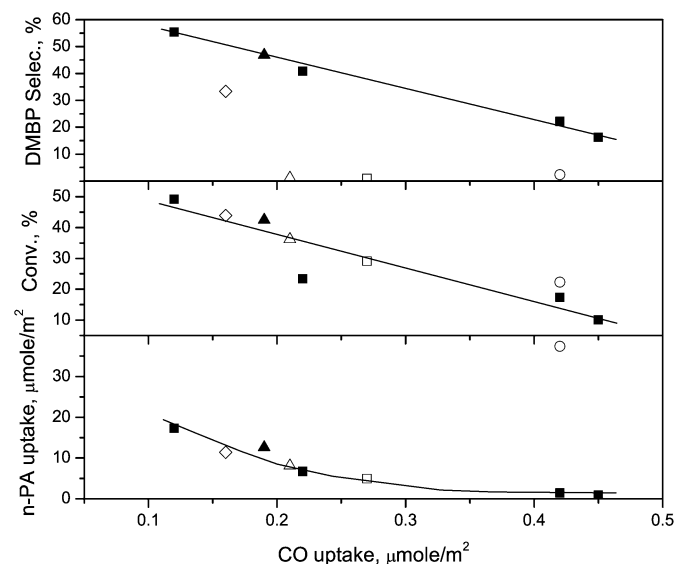


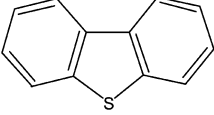
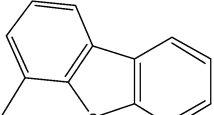
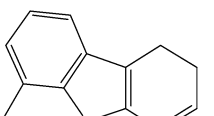
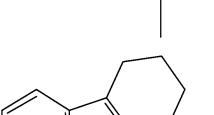
Fig. 9. Conversion of 4,6-DMDBT and selectivity to DMBP over various metal phosphide catalysts at 583 K and 3.0 MPa H₂, plotted as a function of CO uptake: Co_xNi₂P (■), Co_{0.08}MoP (▲), Co₂P (◇) and CoP (○) with MoP (△) and Ni₂P (□) as indicated.

cant shift toward the DDS of 4,6-DMDBT rather than aromatic ring hydrogenation. Isomerization of the 4,6-DMDBT molecule likely occurs, yielding for example, 2,8-DMDBT, which undergoes rapid HDS [30] by DDS.

The distribution of sulfur-containing products (sulfur speciation) obtained with Ni₂P and Co_{0.08}Ni₂P catalysts is compared in Table 5. No 4,6-DMDBT isomerization products were detected, presumably because they underwent rapid DDS on the metal sites of the Co_{0.08}Ni₂P catalyst. Evidence for increased acid-catalyzed methyl cracking on the Co_{0.08}Ni₂P catalyst versus the Ni₂P catalyst is apparent from the data in Table 5, whereas the Ni₂P yielded more hydrogenated product than the Co_{0.08}Ni₂P catalyst. These trends are consistent with the promotion of isomerization of 4,6-DMDBT followed by rapid DDS on the more acidic Co_xNi₂P catalyst versus less isomerization, more hydrogenation, and less DDS on the less acidic Ni₂P catalyst.

The 4,6-DMDBT conversion and DMBP selectivity data are plotted as a function of the CO uptake in Fig. 9. For the Co_xNi₂P series of catalysts, 4,6-DMDBT conversion decreased

Table 5
Comparison of sulfur speciation in liquid product from HDS of 4,6-DMDBT measured at 583 K and 3.0 MPa H₂ over Ni₂P and Co_{0.08}Ni₂P

Product	Comment	Catalyst (mol%)	
		Ni ₂ P	Co _{0.08} Ni ₂ P
	Two methyl groups removed	3	32
	One methyl group removed	24	10
	Partial hydrogenation of one ring	29	18
	Complete hydrogenation of one ring	44	40

with increasing CO uptake. Of more significance, however, is the trend in DMBP selectivity. Fig. 9 shows that as CO uptake increased and *n*-PA uptake decreased, DMBP selectivity decreased. For the Co_xNi₂P catalysts studied herein, maximum selectivity to DMBP occurred on the catalyst with the highest *n*-PA uptake and the lowest CO uptake, that is, the Co_{0.08}Ni₂P catalyst. The data also clearly show that the selectivity behavior of metal phosphides (Co₂P, CoP, MoP, and Ni₂P) differs significantly from that of the Co_xNi₂P and Co_{0.08}MoP catalysts.

4. Discussion

Previous studies of HDS on metal sulfides and phosphides have shown lower DDS selectivity with 4,6-DMDBT as reactant compared with DBT as reactant. Sun et al. [23] reported that on supported NiMoP catalysts over a range of Ni/Mo ratios,

the selectivity to biphenyl was $\geq 80\%$ with DBT as reactant. On $\text{Ni}_2\text{P}/\text{SiO}_2$ and CoP/SiO_2 , Wang et al. [15] reported 100% selectivity to biphenyl with the same reactant, as well as with Ni_xP_y prepared over a wide range of Ni/P ratios during the HDS of DBT [22]. However, with 4,6-DMDBT as reactant, the hydrogenation activity of Ni_2P was 5–7 times greater than the hydrogenolysis (DDS) activity [29]. Similar results were obtained in the present study, with selectivities to the DDS product DMBP $< 3\%$ on Ni_2P , CoP , and MoP . The low selectivity to DDS is due to steric hindrance effects associated with the methyl groups of 4,6-DMDBT [30,31].

An enhanced DDS of 4,6-DMDBT was reported with P_2O_5 addition to conventional metal sulfide catalysts [30]; this effect was attributed to increased Brønsted acidity associated with the added phosphorous, which increased migration of the methyl substituents in the aromatic ring of 4,6-DMDBT. The isomerization would not be important in the HDS of DBT. The products of skeletal isomerization of 4,6-DMDBT have been shown to be much more reactive to DDS than 4,6-DMDBT, especially 2,8-DMDBT [31]. An increase in the DDS rate of 4,6-DMDBT from the addition of P to Mo_2C hydroprocessing catalysts has also been reported [34].

The correlation between the surface phosphorous/metal (P/M) ratio determined by XPS and the ratio of *n*-PA uptake to CO uptake determined by adsorption (Fig. 8) suggests a catalyst surface with Brønsted acid sites associated with phosphate species such as $\text{H}_x\text{PO}_4^{(x-3)}$ and metal sites that chemisorb CO. The source of the Brønsted acid sites is likely a consequence of the incomplete reduction of phosphate species, accentuated by the presence of Co and the catalyst passivation procedure. After reduction of the catalyst precursor by TPR, the catalysts were passivated in diluted O_2 , following procedures known to yield a surface-oxidized overlayer [32]. The P 2p spectra of the passivated catalysts showed the presence of metal phosphide and metal phosphate species for all of the catalysts. $\text{H}_x\text{PO}_4^{(x-3)}$ species, with BEs of 134.3–135.2 eV [33], were not resolved in the XPS spectra, but low concentrations of these species cannot be excluded. The Ni 2p spectra of the Ni_2P and $\text{Co}_{0.08}\text{Ni}_2\text{P}$ catalysts showed two peaks, which were assigned to $\text{Ni}_3(\text{PO}_4)_2$ and Ni_2P . As the Co content increased, a peak assigned to Ni_{12}P_5 and oxidized Ni became evident. Hence it is clear that although the XRD data showed only the presence of bulk metal phosphides, after passivation, both metal phosphide and metal phosphate species were present on the catalyst surface, and in some cases metal oxide was also observed. Before determining the CO uptake, *n*-PA uptake, or activity, the catalysts were pretreated in H_2 by heating to 723 K. However, the TPR data show that, especially in the case of the CoP precursor, a much higher temperature is required for complete reduction to metal phosphide, and, consequently, this pretreatment likely removed only the most reactive surface oxygen. The product water could react with phosphorous species yielding $\text{H}_x\text{PO}_4^{(x-3)}$ and the observed Brønsted acidity. The chemisorption data show that CoP , which had the highest precursor reduction temperature, also had the highest *n*-PA uptake and we assume that this is a consequence of incomplete reduction and more surface phosphate species after passivation. On supported catalysts, the

acidity due to the P may be less important because of reactions between P and the metal oxide support during calcination and reduction [20].

The data of Fig. 9 suggest that the *n*-PA uptake decreased with increasing CO uptake for all of the catalysts but CoP , which had a very high *n*-PA uptake corresponding to the high reduction temperature of the precursor. The 4,6-DMDBT conversion also decreased with increasing CO uptake. The catalyst that gave the highest 4,6-DMDBT conversion and highest DMBP selectivity, $\text{Co}_{0.08}\text{Ni}_2\text{P}$, also had the lowest CO uptake and highest *n*-PA uptake among the $\text{Co}_{0.07}\text{MoP}$ and $\text{Co}_x\text{Ni}_2\text{P}$ catalysts. These results demonstrate the importance of the surface acidity, and hence isomerization, of 4,6-DMDBT for enhanced removal of S by DDS. The data suggest that high selectivity for DDS of 4,6-DMDBT on $\text{Co}_x\text{Ni}_2\text{P}$ and Co_xMoP catalysts was obtained with increasing acid site concentration and decreasing metal site concentration, both of which were determined by the amount of Co added. Note, however, that Co_2P , CoP , Ni_2P , and MoP did not follow the same correlation between DMBP selectivity and CO uptake shown for the $\text{Co}_x\text{Ni}_2\text{P}$ and $\text{Co}_{0.07}\text{MoP}$ catalysts (Fig. 9), indicating that the $\text{Co}_x\text{Ni}_2\text{P}$ catalysts must provide unique acidic and metallic active sites that benefit the DDS route. The $\text{Co}_x\text{Ni}_2\text{P}$ catalysts had larger Ni_2P crystal sizes and BET surface areas than the Ni_2P catalyst. Although we found no direct evidence of a $\text{Co}_x\text{Ni}_2\text{P}$ solid solution, the possibility of a well-dispersed $\text{Co}_x\text{Ni}_2\text{P}$ that is more active for the DDS of 4,6-DMDBT cannot be excluded. Although Co_2P also may be present, it seems less likely that the increased hydrogenolysis activity is associated with an increase in the metallic character of the catalysts. The data of Table 4 show decreasing DMBP selectivity with increasing amounts of Co added to the $\text{Co}_x\text{Ni}_2\text{P}$ catalysts, corresponding to increased CO uptake and XRD patterns showing more metallic phases (Ni_{12}P_5 and Co_2P) present in the bulk. The increased metallic character of the Ni in $\text{Co}_x\text{Ni}_2\text{P}$ with the addition of Co is also indicated by the increase in the Ni 2p peak at a low BE of 852.7 eV, which is assigned to Ni_{12}P_5 [32] but may be associated with Ni(0) [36,37]. However, as this peak intensity increased with Co content, the DMBP selectivity decreased. Although Co_2P has the highest DMBP selectivity among the single-metal phosphides, the TPR data show that this catalyst is more readily reduced than CoP and has a lower acid site density. The XPS data also show that the BE of Co associated with the $\text{Co}_x\text{Ni}_2\text{P}$ catalysts (Fig. 6a) was shifted by about 1.5 eV to higher BE (less metallic and similar to that observed for CoP) compared with the Co associated with Co_2P (778.6 eV).

The significant drop in selectivity observed with increasing addition of Co to the $\text{Co}_x\text{Ni}_2\text{P}$ catalysts suggests that the active phase has a high dispersion only with $x \leq 0.16$. Presumably the $\text{Co}_x\text{Ni}_2\text{P}$ catalysts generate a unique phase, probably a solid solution [25], dispersed on the large Ni_2P crystals, that results in better distribution of acidic and metallic sites and/or provides a catalyst morphology that improves selectivity to DMBP [22].

The P/M ratio as determined by XPS showed significant deviations from the ratio expected based on the catalyst synthesis conditions (Table 3). A P-enriched surface for all of the $\text{Co}_x\text{Ni}_2\text{P}$ catalysts compared to Ni_2P was observed. Further-

more, the change in P/M surface composition as determined by XPS, was consistent with the CO chemisorption data and the *n*-PA temperature-programmed desorption data. As shown in Fig. 8, the P/M atom ratio was well correlated with the *n*-PA/CO uptake ratio. If one assumed that the Brønsted acidity resided in $H_xPO_4^{(x-3)}$ species, and that all of the surface P was in this form with $x = 3$, then the slope of the line shown in Fig. 8 would be expected to be 1/3, assuming an adsorption stoichiometry of 1:1 for *n*-PA/Brønsted acid site and CO uptake/metal site. However, the slope of the line in Fig. 8 is 10 times smaller than this, suggesting a much lower CO uptake than available surface metal sites as determined by XPS. (Note that the XPS data indicate that some of the surface P is present as metal phosphide, which would tend to increase the slope of the line of Fig. 8.) The limitation of CO adsorption to titrate the metal sites on metal phosphides has been discussed in the literature [15,20,23], and the present study supports the conclusion the CO adsorption underestimates the metal sites in these metal phosphide catalysts.

5. Conclusion

In the present study, the addition of ca. 3 mol% Co to Ni₂P and MoP resulted in a significant increase in DDS selectivity during 4,6-DMDBT conversion. The change in selectivity corresponded to various observed changes in the catalyst properties, particularly surface Brønsted acidity and metal sites as determined by *n*-PA adsorption and CO adsorption, respectively. The most selective catalyst for DDS of 4,6-DMDBT was the Co_{0.08}Ni₂P catalyst, which had the lowest CO uptake and highest *n*-PA uptake among the Co_{*x*}Ni₂P and Co_{0.07}MoP catalysts studied.

Acknowledgments

Financial support from the Natural Sciences and Engineering Research Council of Canada is gratefully acknowledged. I.A. thanks the Canadian Commonwealth Scholarship and Fellowship Program and the Government of Ghana for financial aid.

References

- [1] C. Song, M. Xiaoliang, Appl. Catal. B 41 (2003) 207.
- [2] T. Kabe, A. Ishihara, W. Qian, Hydrodesulfurization and Hydrodenitrogenation, Wiley-VCH, Weinheim, 1999.

- [3] X. Tiancum, W. Hariato, D. Jianwen, K.S. Coleman, M.L.H. Green, J. Catal. 211 (2002) 183.
- [4] L. Senzi, L. Jae, J. Catal. 173 (1998) 134.
- [5] C.W. Colling, L.T. Thompson, J. Catal. 146 (1994) 193.
- [6] S. Krysztof, H.S. Kim, C. Sayag, D. Brodzki, G. Djega-Mariadassou, Catal. Lett. 53 (1998) 59.
- [7] S. Ramanathan, C.C. Yu, S.T. Oyama, J. Catal. 173 (1998) 10.
- [8] R. Prins, G. Pirngruber, T. Weber, Chimia 55 (2001) 791.
- [9] W. Li, B. Dhandapani, S.T. Oyama, Chem. Lett. 207 (1998) 207.
- [10] S.T. Oyama, P. Clark, L.S. Teixeira da Siva, E.J. Lede, F.G. Requejo, J. Phys. Chem. 105 (2001) 4961.
- [11] P. Clark, W. Li, S.T. Oyama, J. Catal. 200 (2001) 140.
- [12] C. Stinner, R. Prins, Th. Weber, J. Catal. 191 (2000) 434.
- [13] D.C. Phillips, S.J. Sawhill, R. Self, M.E. Bussell, J. Catal. 20 (2002) 266.
- [14] S.T. Oyama, J. Catal. 216 (2003) 343.
- [15] X. Wang, P. Clark, S.T. Oyama, J. Catal. 208 (2002) 321.
- [16] S.T. Oyama, X.T. Wang, F.G. Requejo, T. Sato, Y. Yoshimura, J. Catal. 209 (2002) 1.
- [17] V. Zuzaniuk, R. Prins, J. Catal. 219 (2003) 85.
- [18] C. Stinner, R. Prins, Th. Weber, J. Catal. 202 (2001) 187.
- [19] S.J. Sawhill, D.C. Phillips, M.E. Bussell, J. Catal. 215 (2003) 208.
- [20] P.A. Clark, S.T. Oyama, J. Catal. 218 (2003) 78.
- [21] L.R. Wang, Y. Teng, X. Li, M. Lu, J. Ren, Y. Wang, Y. Hu, J. Catal. 229 (2005) 314.
- [22] S.T. Oyama, X. Wang, Y.K. Lee, K. Band, F.G. Requejo, J. Catal. 210 (2002) 207.
- [23] F. Sun, W. Wu, Z. Wu, J. Guo, Z. Wei, Y. Yang, Z. Jiang, F. Tian, C. Li, J. Catal. 228 (2004) 298.
- [24] J.A. Rodriguez, J.Y. Kim, J.C. Hanson, S.J. Sawhill, M.E. Bussell, J. Phys. Chem. B 107 (2003) 6276.
- [25] D. Ma, T. Xiao, S. Xie, W. Zhou, S.L. Gonzalez-Cortes, M.L.H. Green, Chem. Mater. 16 (2004) 2697.
- [26] L.S. Dake, D.R. Baer, D.M. Friedrich, J. Vac. Sci. Technol. A 7 (1989) 1634.
- [27] R. Gresch, W. Mueller-Warmuth, H. Dutz, J. Non-Cryst. Solids 34 (1979) 127.
- [28] R. Franke, Th. Chasse, P. Streube, A. Meisel, J. Electron Spectrosc. Relat. Phenom. 56 (1991) 381.
- [29] J.H. Kim, X. Ma, C. Song, S.T. Oyama, ACS Div. Fuel Chem. Prepr. 48 (1) (2003) 40.
- [30] C. Kwak, M.Y. Kim, K. Choi, S.H. Moon, Appl. Catal. 185 (1999) 19.
- [31] T. Isoda, Y. Takase, K. Kusakabe, S. Morooka, Energy Fuels 14 (2000) 585.
- [32] S.J. Sawhill, K.A. Layman, D.R. Van Wyk, M.H. Engelhard, C. Wang, M.E. Bussell, J. Catal. 231 (2005) 300.
- [33] E. Fluck, D. Weber, Z. Naturforsch. B 29 (1974) 603.
- [34] J.-M. Manoli, P. Da Costa, M. Brun, M. Vrinat, F. Maugé, C. Potvin, J. Catal. 221 (2004) 365.
- [35] E.E. Khwaja, M.A. Salim, M.A. Khan, F.F. Al-Adel, G.D. Khattak, Z. Hussain, J. Non-Cryst. Solids 33 (1989) 110.
- [36] J.C. Klein, D.M. Hercules, J. Catal. 82 (1983) 424.
- [37] C.R. Anderson, R.N. Lee, J.F. Morar, R.L. Park, J. Vac. Sci. Technol. 20 (1982) 617.